Journal of Water Process Engineering 15 (2017) 2–17

Contents lists available at ScienceDirect

Journal of Water Process Engineering

journal homepage: www.elsevier.com/locate/jwpe

Synthesis of cryptocrystalline magnesite–bentonite clay composite and its application for neutralization and attenuation of inorganic contaminants in acidic and metalliferous mine drainage

Vhahangwele Masindi[c,*], Mugera W. Gitari[a], Hlanganani Tutu[b], Marinda DeBeer[d]

[a] Environmental Remediation and Water Pollution Chemistry Research Group, Department of Ecology and Resources Management, School of Environmental Science, University of Venda, P/bag X5050, Thohoyandou 0950, South Africa
[b] Molecular Sciences Institute, School of Chemistry, University of the Witwatersrand, P/Bag X4, WITS, 2050 Johannesburg, South Africa
[c] CSIR (Council of Scientific and Industrial Research), Built Environment, Building Science and Technology (BST), P.O Box 395, Pretoria 0001, South Africa
[d] DST/CSIR National Centre for Nano-Structured Materials, Council for Scientific and Industrial Research, P.O. Box 395, Pretoria 0001, South Africa

ARTICLE INFO

Article history:
Received 23 April 2015
Received in revised form
12 November 2015
Accepted 22 November 2015
Available online 18 December 2015

Keywords:
Acid mine drainage
Neutralization
Magnesite–bentonite clay composite
Inorganic contaminants
Adsorption modelling

ABSTRACT

The primary aim of this study was to synthesize cryptocrystalline magnesite–bentonite clay composite by mechanochemical activation and evaluate its usability as low cost adsorbent for neutralization and attenuation of inorganic contaminants in acidic and metalliferous mine drainage. The composite was synthesized at 1:1 weight to weight ratio. The capacity of the composite to neutralize acidity and remove toxic chemical species from synthetic and field AMD was evaluated at optimized conditions. Interaction of the composite with AMD led to an increase in pH (pH > 11) and lowering of metal concentrations. The removal of chemical species was optimum at 20 min of equilibration and 1 g of dosage. The composite removed ≈99% (Al^{3+}, Fe^{3+}, and Mn^{2+}) and ≈90% (SO_4^{2-}) from raw mine effluent. Adsorption kinetics fitted better to pseudo-second-order kinetic than pseudo-first-order kinetic hence confirming chemisorption. Adsorption data fitted better to Freundlich adsorption isotherm than Langmuir hence confirming multisite adsorption. Gibbs free energy model predicted that the reaction is spontaneous in nature for Al, Fe and sulphate except for Mn. Geochemical model indicated that Fe was removed as $Fe(OH)_3$, goethite, and jarosite, Al as basaluminite, boehmite and jurbanite, $Al(OH)_3$ and as gibbsite and diaspore. Al and Fe precipitated as iron (oxy)-hydroxides and aluminium (oxy)-hydroxides. Mn precipitated as rhodochrosite and manganite. Ca was removed as gypsum. Sulphate was removed as gypsum, and Fe, Al hydroxyl sulphate minerals. Mg was removed as brucite and dolomite. It was concluded that the composite has the potential to neutralize acidity and attenuate potentially toxic chemical species from acidic and metalliferous mine drainage.

1. Introduction

Acidic and metalliferous drainage originating from metal mining activities can cause serious environmental pollution [1]. On release to receiving aquatic ecosystems, acid mine drainage (AMD) can cause major ecological impacts which have the capability to compromise the integrity of terrestrial and aquatic ecosystems to sustain life [2]. In South Africa, AMD is generated by oxidation of pyrite associated with coal and gold seams [3]. During mining processes, pyrite is exposed to water and oxygen and this promotes the formation of AMD post oxidation [4]. During rainfall on tailings dumps and rising groundwater in disused mineshafts, water and oxygen interacts with pyrite leading to the formation of acidic effluent. The resultant acidic water accelerates leaching of metals from surrounding rock strata or tailings [2]. The release of metals to effluent waters makes the water metalliferous. In most instances, the formation of AMD can be represented by the following chemical equations [5]:

$$2FeS_{2(s)} + 7O_{2(g)} + 2H_2O \xrightarrow{bacteria} 2Fe^{2+}_{(aq)} + 4H^{+}_{(aq)} + 4SO^{2-}_{4(aq)} \quad (1)$$

$$4Fe^{2+}_{(aq)} + O_{2(g)} + 4H^{+}_{(aq)} \rightarrow 4Fe^{3+}_{(aq)} + 2H_2O_l \quad (2)$$

$$FeS_{2(s)} + 14Fe^{3+} + 8H_2O \rightarrow 15Fe^{2+} + 2SO^{2-}_{4(l)} + 16H^{+} \quad (3)$$

* Corresponding author.
E-mail addresses: VMasindi@csir.co.za, masindivhahangwele@gmail.com (V. Masindi).

http://dx.doi.org/10.1016/j.jwpe.2015.11.007
2214-7144/

$$Fe^{3+}_{(aq)} + 3H_2O_l \rightarrow Fe(OH)_{3(s)} + 3H^+_{(aq)} \quad (4)$$

These reactions are also mediated by bacteria (Eq. (1)) [6]. Acidic and metalliferous drainage is a prime issue of environmental concern since it causes a reduction in biodiversity and loss of authentic value of pristine ecosystems [1]. Acid mine drainage is characterised by high acidity and elevated concentrations of Al, Fe, Mn and SO_4^{2-}. In addition, it also contains trace amounts of As, B, Cr, Cu, Co, Mo, Ni, Pb, Se, and Zn [3,7]. This mine effluent needs to be contained and treated before discharge to natural water bodies [1]. Several technologies have been developed for treatment of AMD and these include ion-exchange [8], adsorption [9], precipitation [10], and phytoremediation [11]. Maree and Du Plessis [12] have evaluated the use of limestone for treatment of acid mine drainage. Biological agents were also used for removal of sulphates from acid mine drainage as a polishing step [13]. Due to cost implications, inefficient treatment, selective treatment and generation of toxic sludge, the existing technologies have limitation and companies are in constant search for sustainable AMD treatment and management technologies [14]. To date, limestone has been used for AMD treatment but has limitations of raising the pH to a maximum of 7 which is not sufficient to remove all metal pollutants in AMD, and additional liming is necessary, thus making it unsustainable [15,16]. Moreover limestone treatment leads to generation of huge amounts of sludge that has to be managed. South African bentonite clay has been evaluated for AMD treatment in a recent study by Gitari [5] but was observed to have low metal removal efficiency especially at high concentrations and could only increase the pH of the reaction mixture ≈4 which is not sufficient for precipitation of metal species.

Clay have excellent physicochemical such as high adsorption capacities, ion exchange capacities, swelling properties, surface area, leafy or lamella structure, abundance and low cost [17–22]. Clay minerals have also received great attention as alternative material for decontamination of polluted waterbodies. In addition, these materials are environmentally friendly, abundant, versatile and readily available making their application economically sustainable [23]. Techniques such as intercalation and pillaring [24,18], acid activation [25,26] and mechanochemical activation [27] can be employed in an attempt to improving the adsorption and inorganic contaminants removal properties of the clays. The preparation of organoclays by grafting and direct synthesis has also been used for metals retention [27].

Amongst all clay modifications and composite synthesis science, mechanochemical activation was reported to present good responses because it is cheap, economically viable and, environmentally friendly technique of modification. Documented literatures have meticulously described the influence of mechanochemical activation on the morphological and microstructural alterations and improvements of the clay [28,26], but only a limited number of research studies have investigated the use of mechanical milling on their adsorption and reactivity properties [26,29,30]. Moreover, a study by Gitari [5] observed that bentonite clay being a geological material possessed free alkaline materials that can be released on mechanochemical activation and be available to increase the pH of the reaction mixture. Fragmentation, distortion, breakage of crystalline networks and cobwebs, and particle size reduction followed by an increase of the surface area, exfoliation of particles and amorphization, can lead to the increase of the removal efficiencies of the pollutants on fabricated composites [31,27].Clay has been widely used for removal of inorganic and organic contaminants from aqueous systems [32]. The main mode of metals attenuation by clay is adsorption [33]. Adsorption of inorganic chemical species on clay minerals is highly pH dependent, thus, limiting their application in wastewater amelioration (pH < 4) [26]. In an attempt to counter for the limitations in the use of the raw and modified clays as adsorbents, the adsorbents can be prepared in a composite form with some metal oxides [26] and carbonates [34]. To respond to the challenges that are being presented by current technologies, government, mining houses, and scientific communities are seeking innovative and locally available technologies for remediating AMD.

To the authors' knowledge, the investigation of mechanochemically synthesized bentonite clay–cryptocrystalline magnesite composite as adsorbent for simultaneous neutralization and attenuation of metal species and sulphate has never been reported before. The purpose of this study was to synthesize a magnesite–bentonite clay composite adsorbent and evaluate its ability to neutralize acidity and remove metal species and sulphate from metalliferous mine drainage in a single process step.

2. Materials and methods

2.1. Sampling

Raw magnesite rocks from the Folovhodwe Magnesite Mine in Limpopo Province, South Africa, were collected without any prior processing. Bentonite clay was supplied by ECCA (Pty) Ltd. (Cape Town, South Africa). Raw AMD samples were collected from a disused mine shaft near Krugersdorp, Gauteng Province, South Africa.

2.2. Preparation of cryptocrystalline magnesite and bentonite clay

Magnesite rock samples were milled to a fine powder (Retsch RS 200 mill) and sieved (32 μm particle sizes). The raw bentonite was washed by soaking in ultra-pure water and draining after 10 min. The ultrapure water used was such that it covered the entire sample in the beaker and was allowed to overflow. The procedure was repeated four times. The washed bentonite was dried for 24 h at 105 °C. The dried samples were milled into a fine powder (Retsch RS 200 mill) and sieved (32 μm particle size sieves).

2.3. Composite preparation

Mechanochemical synthesis was used as a method for the preparation of the clay composite. A vibratory ball-mill was used for making the porous magnesite–bentonite clay composite. Powdered bentonite (500 g) and magnesite (500 g) were mixed on a 1:1 wt% mass ratio. The mixture was crushed and homogenised by pulverizing into a fine powder (Retsch RS 200 mill) for 30 min at 1600 rpm. After sieving to <32 μm particle size, the material was kept in sealed plastic bags (Zip-lock). The parameters for milling were previously determined as optimal milling parameters for mechanochemical modification of bentonite clay–cryptocrystalline magnesite composite [34]

2.4. Simulated AMD

Synthetic acid mine drainage (SAMD) was used for experimentation as real AMD is extremely difficult to work with in optimization due to oxidation and hydrolysis on exposure to the open leading to rapid changes in chemistry. A simplified solution containing the major ions found in AMD was prepared as described by Tutu et al. [3], Gitari et al. [35], Masindi et al. [36,30,37] and Potgieter-Vermaak et al. [38].

The composition of SAMD used in this study is shown in Table 1. AMD was simulated by dissolving the following quantities of salts in 1000 mL of Milli-Q ultra-pure water (18MΩ), 7.48 g $Fe_2(SO_4)_3.H_2O$, 2.46 g $Al_2(SO_4)_3 \cdot 18H_2O$, and 0.22 g $MnCl_2$ to give a solution of 2000 mg/L Fe^{3+}, 200 mg/L Al^{3+} and 100 mg/L Mn^{2+}. An aliquot of

Table 1
SAMD used in this study [36,30,37].

Salt dissolved	Species	Concentration
$Al_2(SO_4)_3{\cdot}18H_2O$	Al^{3+}	200 mg/L
$Fe_2(SO_4)_3{\cdot}H_2O$	Fe^{3+}	2000 mg/L
$MnCl_2$	Mn^{2+}	100 mg/L
H_2SO_4 and Al and Fe salts	SO_4^{2-}	6250 mg/L

5 mL of 0.05 M H_2SO_4 was added to make up the SO_4^{2-} concentration to 6250 mg/L. The salts were dissolved in 1000 mL volumetric flasks. The pH of the solution was <3. For the batch experiments, the working solutions were prepared from these stock solutions by appropriate dilutions.

2.5. Characterization of aqueous solution

pH, total dissolved solids (TDS) and electrical conductivity (EC) were monitored using CRISON MM40 portable pH/EC/TDS/Temperature multimeter probe. Aqueous samples were analysed using ICP-MS (7500ce, Agilent, Alpharetta, GA, USA) for metal cations while sulphate was analysed using IC (850 professional IC Metrohm, Herisau, Switzerland). The accuracy of the analysis was monitored by analysis of National Institute of Standards and Technology (NIST) water standards [30].

2.6. Mineralogical, chemical and microstructural characterisation

Mineralogical composition of composite and resulting solid residues was determined using XRD, Analyses were performed by using a Philip PW 1710 diffractometer equipped with graphite secondary monochromatic. Elemental composition was determined using XRF, the Thermo Fisher ARL-9400 XP+ Sequential XRF with WinXRF software. XRF and XRD were done at the University of Pretoria, South Africa. Morphology was determined using SEM–EDS (JOEL JSM-840, Hitachi, Tokyo, Japan), surface area and porosity were determined using BET (Micromeritics Tristar II, Norcross, GA, USA). pH_{PZC} was determined using solid addition method [17].

2.7. Experimental procedures

To determine the optimum condition for AMD treatment, several operational parameters were optimized and they include: effect of solid to liquid ratios, shaking time, composite dosage, and species concentrations. All experiments were performed in triplicate and the data averaged.

2.7.1. Effect of cryptocrystalline magnesite: bentonite clay ratios

The effect of cryptocrystalline magnesite contents on neutralization and attenuation of metal species and sulphate was assessed. Portions of 100 mL solutions of SAMD were pipetted into 250 mL flasks into which 1 g of the composite samples were added. The magnesite to bentonite clay (wt%) was varied as follow: 0.1:1, 0.2:1, 1:1, 2:1, 3:1, 4:1. The mixture was equilibrated for 60 min on a reciprocating shaker. The initial pH of the working solutions was <3. After shaking, the mixture was filtered through a 0.45 μm pore nitrate cellulose filter membrane. The filtrates were preserved by adding two drops of concentrated HNO_3 acid to prevent ageing and immediate precipitation of Al, Fe and Mn and refrigerated at 4 °C prior to analysis by an inductively coupled plasma mass spectrometer (ICP-MS) (7500ce, Agilent, Alpheretta, GA, USA). The pH before and after agitation was measured using the CRISON multimeter probe (model MM40). A separate set was left un-acidified for sulphate analysis by Ion Chromatograph (850 professional IC Metrohm, Herisau, Switzerland).

2.7.2. Effect of time

Portions (100 mL) each of SAMD were pipetted into 250 mL flasks into which 1 g of the composite samples were added. The mixtures were then equilibrated for 1, 10, 20, 60, 120, 180, 240, 300 and 360 min at 250 rpm using the Stuart reciprocating shaker. The pH, metal species and sulphate contents were determined as described in the preceding section.

2.7.3. Effect of dosage

Portions (100 mL) each of SAMD were pipetted into 250 mL flasks and varying masses (0.1–8 g) of the composite were added into each flask, respectively. The mixtures were agitated using a shaker for an optimum time of 30 min at 250 rpm. The pH, metal species and sulphate contents were determined as described in the preceding section.

2.7.4. Effect of species concentration

To investigate the effects of adsorbate concentration on reaction kinetics, several dilutions were made from the simulated AMD stock solution. The pHs of the simulated AMD were not adjusted. The capacity of the adsorbent to neutralize and attenuate metal concentrations from aqueous solution was then assessed by increasing metal concentrations. Solutions of 100 mL each containing 100–2000 mg/L Fe^{3+}; 10–200 mg/L Al^{3+}; 5–100 mg/L Mn^{2+} and 300–6250 mg/L SO_4^{2-} were prepared in triplicate and 1 g of the composite was added to each sample container. The mixtures were equilibrated by shaking for 30 min. The initial pH of the working solutions was <3. The pH, metal and sulphate contents were determined as described in the preceding section.

2.7.5. Treatment of field AMD at optimized conditions

Field AMD samples were treated at established optimized conditions in order to assess the effectiveness of magnesite–bentonite clay composite treatment. The pH and metal species contents were determined as described previously while a separate set of samples was left un-acidified for SO_4^{2-} analysis. Metal species were assayed using ICP-MS, pH, EC and TDS were measured as described previously. The resultant solid residue, after contact with AMD, was characterized in order to gain an insight into the fates of chemical species after magnesite–bentonite clay composite treatment.

2.8. Calculation of metal species, sulphate removal and adsorption capacity

Percentage removal and adsorption capacity were evaluated using Eqs. (5) and (6) [30].

$$\text{Percentage removal}\,(\%) = \left(\frac{C_i - C_e}{C_i}\right) \times 100 \tag{5}$$

$$\text{Adsorption capacity}(q_e) = \frac{(C_i - C_e)\,V}{m} \tag{6}$$

where C_i = initial concentration, C_e = equilibrium ion concentration, V = volume of solution; m = mass of the composite.

2.9. Adsorption Kinetics

Adsorption kinetics were evaluated using pseudo-first-order, second order kinetics and Intraparticle diffusion model [39]. A Lagergren pseudo first order kinetic model is a well-known model that is used to describe mechanisms of metal species adsorption by an adsorbent. It can be written as follow [40]:

$$\ln(q_e - q_t) = \ln q_e - k_1 t \tag{7}$$

where k_1 (min^{-1}) is the pseudo-first-order adsorption rate coefficient and q_e and q_t are the values of the amount adsorbed per unit

mass at equilibrium and at time t, respectively. The pseudo-second-order kinetic model is another kinetic model that is widely used to describe the adsorption process from an aqueous solution. The linearized form of the pseudo-second-order rate equation is given as follow [41]:

$$\frac{t}{qr} = \frac{1}{k_2 q_e^2} + \frac{t}{q_e} \tag{8}$$

where k_2 [g (mg min^{-1})] is the pseudo-second-order adsorption rate coefficient and q_e and q_t are the values of the amount adsorbed per unit mass at equilibrium and at time t, respectively. The overall kinetics of the adsorption from solutions may be governed by the diffusional processes as well as by the kinetics of the surface chemical reaction. In diffusion studies, the rate is often expressed in terms of the square root time [30].

$$q_t = k_{id} t^{1/2} + C_i \tag{9}$$

where k_{id} (mg g^{-1} min$^{-1/2}$) is the Intraparticle diffusion coefficient (slope of the plot of q_t vs. $t^{1/2}$) and C_i is the Intraparticle diffusion rate constant. Parameters were calculated to determine whether film diffusion or Intraparticle diffusion is the rate limiting step. The model suggested that if the sorption mechanism is via Intraparticle diffusion then a plot of qt versus $t^{1/2}$ will be linear; and Intraparticle diffusion is the sole rate-limiting step when such a plot passes through the origin. When the sorption process is controlled by more than one mechanism, then a plot of qt versus $t^{1/2}$ will be multi-linear.

2.9. Adsorption isotherms and thermodynamics

Adsorption isotherms were evaluated using Langmuir and Freundlich adsorption models [39]. Thermodynamics evaluations were done using Gibbs free energy model [42]. The most important model of monolayer adsorption came from Langmuir. This isotherm is given as follows [29]:

$$q_e = \frac{Q_0 b C_e}{1 + b C_e} \tag{10}$$

The constant Q_0 and b are characteristics of the Langmuir equation and can be determined from a linearized form of Eq. (11). The Langmuir isotherm is valid for monolayer sorption due to a surface with finite number of identical sites and can be expressed in the following linear form [21]:

$$\frac{C_e}{Q_e} = \frac{1}{Q_m b} + \frac{C_e}{Q_m} \tag{11}$$

The essential characteristics of the Langmuir isotherm can be expressed in terms of a dimensionless constant separation factor or equilibrium parameter, R_L, which is defined as [20]:

$$R_L = \frac{1}{1 + b C_o} \tag{12}$$

where C_e = equilibrium concentration (mg L^{-1}), q_e = amount adsorbed at equilibrium (mg g^{-1}), Q_m = Langmuir constants related to adsorption capacity (mg g^{-1}) and b = Langmuir constants related to energy of adsorption (L mg^{-1}). A plot of C_e versus C_e/Q_e should be linear if the data conforms to the Langmuir isotherm. The value of Q_m is determined from the slope and the intercept of the plot. It is used to derive the maximum adsorption capacity and b is determined from the original equation and represents the degree of adsorption.

The Freundlich adsorption isotherm describes the heterogeneous surface energy by multilayer adsorption. The Freundlich isotherm is formulated as follows [30]:

$$q_e = k {C_e}^{1/n} \tag{13}$$

The equation may be linearized by taking the logarithm of both sides of the equation and can be expressed in linear form as follows [30]:

$$\log\ q_e = \frac{1}{n} \log C + \log K \tag{14}$$

where C_e = equilibrium concentration (mg L^{-1}), q_e = amount adsorbed at equilibrium (mg g^{-1}), K = Partition Coefficient (mg g^{-1}) and n = degree of adsorption. A linear plot of log C_e versus log q_e indicates whether the data is described by the Freundlich isotherm. The value of K implies that the energy of adsorption on a homogeneous surface is independent of surface coverage and n is an adsorption constant which reveals the rate at which adsorption is taking place. In order to fully understand the nature of adsorption the thermodynamic parameters such as free energy change (ΔG) could be calculated. It was possible to estimate these thermodynamic parameters for adsorption reaction by considering the equilibrium constant under the experimental conditions. The Gibbs free energy change of adsorption was calculated using the following equation:

$$\Delta G = -RT \ln K_c \tag{15}$$

where R is gas constant (8.314 J mg^{-1} K^{-1}), T is temperature and K_c is the equilibrium constant ($K_c = q_e/c_e$). The positive ΔG value indicates that the sorption process is spontaneous in nature and also feasible whereas the negative value indicates that the reaction is not spontaneous and feasible.

An error analysis was required to evaluate the fit of the adsorption isotherms to experimental data. In the present study, the linear coefficient of determination (R^2) was employed for the error analysis. The linear coefficient of determination was calculated by using the Eq. (16) [43]:

$$r = \frac{n\Sigma xy - (\Sigma x)(\Sigma y)}{\sqrt{n(\Sigma x^2) - (\Sigma x)^2} - \sqrt{(\Sigma y^2) - (\Sigma y)^2}} \tag{16}$$

Theoretically, the R^2 value varies from 0 to 1. The R^2 value shows the variation of experimental data as explained by the regression equation. In most studies, the coefficient of determination, R^2, was applied to determine the relationship between the experimental data and the kinetics or isotherms.

2.10. Geochemical modelling

To complement chemical solution and physicochemical characterization results, the ion association model PHREEQC was used to calculate ion activities and saturation indices of mineral phases based on the pH and solution concentrations of major ions in supernatants that were analysed after the optimized conditions. Mineral phases that were likely to form during treatment of AMD with magnesite–bentonite clay composite were predicted using the PHREEQC geochemical modelling code using the WATEQ4F database [44]. Species which are more likely to precipitation was determined using saturation index (SI). In this case, SI < 1 = under saturated solution, SI = 1 = saturated solution and SI > 1 = supersaturated solution [37].

3. Results and discussion

3.1. X-ray diffraction (XRD) analysis

The mineralogical composition of magnesite (1), bentonite clay (2), composite (3) and AMD-reacted composite (4) are shown in Fig. 1.

XRD analysis showed that magnesite consists of magnesite, periclase, brucite, quartz and forsterite as the main mineral phases.

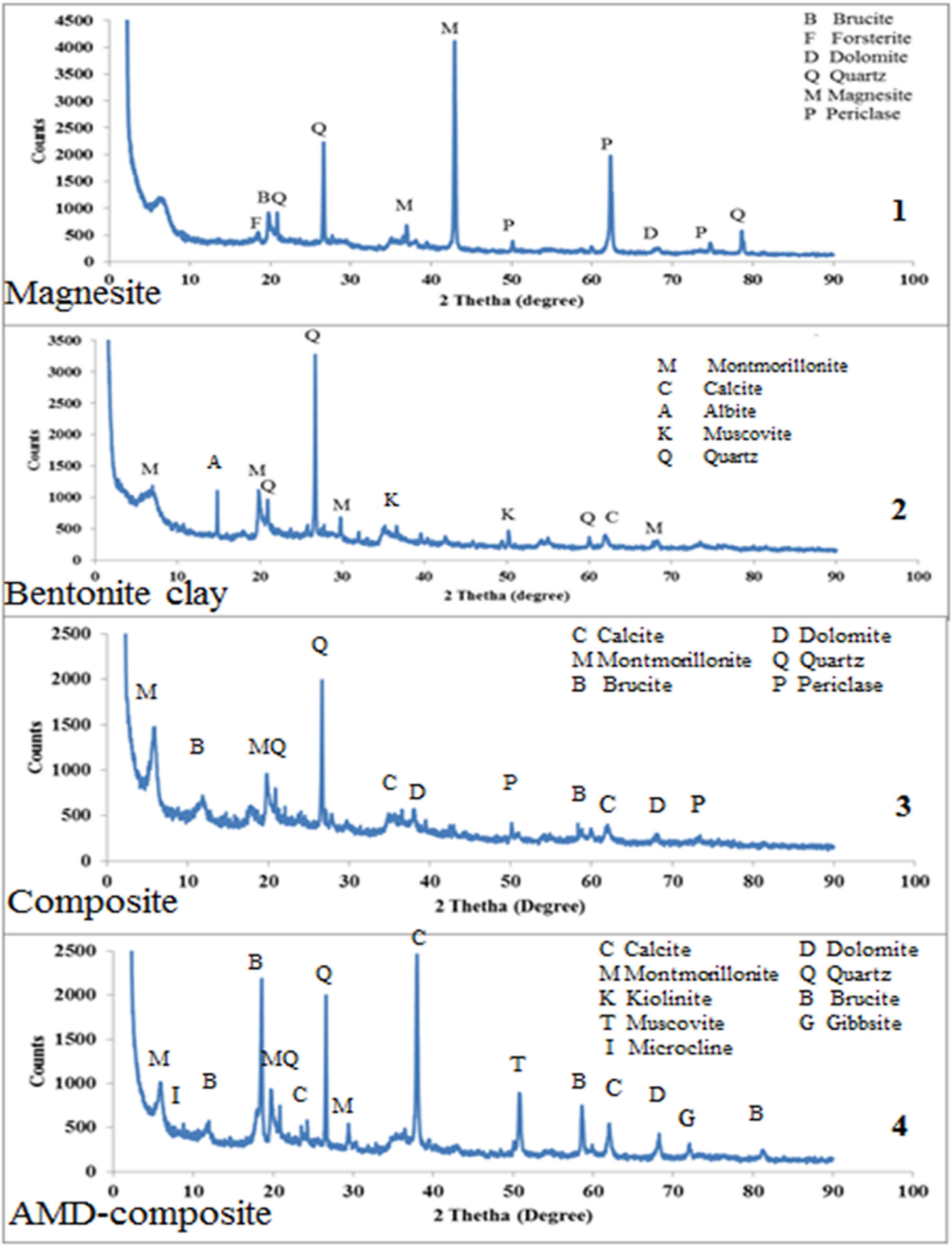

Fig. 1. XRD patterns of cryptocrystalline magnesite (1), bentonite clay (2), composite (3) and AMD-reacted composite (4).

Table 2
Compositions of raw and AMD-reacted composite.

Composition	Raw composition (wt.%)	AMD-reacted composite (wt.%)
SiO_2	30	27
Al_2O_3	7	6
Fe_2O_3	2	4
MnO	0	1
MgO	51	37
CaO	2	4
Na_2O	1	0.4
K_2O	1	0.4
SO_3	1	5
LOI	3	12.2
H_2O-	2	3
Total	100	100

Table 3
Trace elemental composition of raw and reacted composite.

Elements (mg L^{-1})	Raw composite	AMD-reacted composite
As	<4	10
Ba	<5	99
Br	16	<2
Ce	<10	29
Co	1.2	1.2
Cr	6.9	8.6
Cs	104	<5
Cu	7.6	5.7
Ga	8.3	8.7
Hf	6	<3
La	<10	12
Mo	13	<2
Nb	163	8.6
Nd	35	16
Ni	79	80
Pb	11	14
Rb	<2	5.5
Sc	<3	3.5
Se	445	<1
Sm	17	<10
Sr	33	41
Ta	18	<2
Th	5.3	8.6
Tl	4.2	<3
Y	11	9
Zn	8.2	19
Zr	<2	60

Bentonite clay was observed to contain montmorillonite, quartz, calcite and muscovite. The composite was reported to contain montmorillonite, quartz, dolomite, calcite, brucite, periclase and muscovite. The mechanochemical synthesis of the bentonite clay in the presence of cryptocrystalline magnesite led to an amorphization of the magnesite and bentonite clay in the composite that was revealed through widening, as well as the reduction in the number and intensity of the reflection [Fig. 1(3)]. AMD-reacted composite was observed to be constituted of montmorillonite, kaolinite, microcline, quartz, dolomite, brucite, calcite, gibbsite and muscovite [Fig. 1(4)].

Table 5
Different kinetic model parameters for adsorption of Mn, Al, Fe and sulphate on the composite.

Pseudo-first-order kinetic model

Element	$q_{e,exp}$ (mg g^{-1})	$q_{e,calc}$ (mg g^{-1})	K_1	R^2
Mn	9.99	−11.12	0.177	0.94
Al	19.99	−4.77	0.309	0.99
Fe	199.9	−8.94	0.331	0.91
Sulphate	521.1	−6.99	1.519	0.90

Pseudo-second-order kinetic model

Eement	$q_{e,exp}$ (mg g^{-1})	$q_{e,calc}$ (mg g^{-1})	K_2	R^2
Mn	9.99	10.01	3.67	1
Al	19.99	20.04	1.24	1
Fe	199.9	200	1.67	1
Sulphate	521.1	526.3	0.69	0.999

Intraparticle diffusion model

Element	$q_{e,exp}$ (mg g^{-1})	C_i (mg g^{-1})	K_{id} (mg g^{-1} $min^{-1/2}$)	R^2
Mn	9.99	2.85	13.93	0.48
Al	19.99	2.20	2.89	0.18
Fe	199.9	1.02	0.35	0.29
Sulphate	521.1	−0.06	0.05	0.17

3.2. X-ray fluorescence (XRF) analysis

The compositions of raw and AMD-reacted composite are shown in Tables 2 and 3.

Bentonite clay is mainly comprised of Al and Si confirming that the material under study is an alumino-silicate. The presence of Fe, Mg, Ca, Na and K on clay interlayers is indicating that these are the main exchangeable cations in bentonite clay matrices. Availability of Mg, Ca, Na and K will aid in the neutralisation of AMD. Magnesite is dominated by MgO. These results corroborated results obtained by [45] that cryptocrystalline magnesite is composed of close to 90% of MgO. The composite was dominated by Al, Mg and Si hence showing that the material is a combination of magnesite and a clay mineral (Table 2) . After contacting AMD with the composite, there was a drastic reduction in Na and K on the composite matrices. This may be described by an increase in Na and K is product water post treatment. Ca, SO_3, Mn and Fe were observed to increase in the secondary residue. This may be better explained by reduction of those chemical species in treated AMD (Table 8). Notable reduction in Na, K and Mg indicate that these are the exchangeable elements on composite galleries. After interaction with AMD, the resultant solid residue was shown to be enriched with chemical species that are prevalent in AMD, showing that the composite was scavenging chemical species from AMD.

Traces of Co, Cr, Cu, Ni, Pb and Zn were observed to be present in the secondary residues post treatment of AMD. This indicates that those elements were removed from AMD to secondary residues. Trace elements (Table 3) were also observed to be present at notable

Table 4
Surface area for magnesite, bentonite clay, magnesite–bentonite clay composite and AMD-reacted composite.

Parameters	Magnesite	Bentonite clay	Composite	AMD-composite
Surface area (m^2/g)				
Single point surface area	16.64	37.05	18.33	15.94
BET surface area	16.76	37.21	18.36	16.17
Adsorption cumulative surface area pore	10.67	20.32	10.57	12.58
Pore volume (cm^3/g)				
Single point pore volume	0.079	0.08	0.07	0.072
Cumulative volume of pores	0.099	0.08	0.09	0.083
Pore size (nm)				
Adsorption average pore width	18.80	8.98	15.75	17.78
Adsorption average pore diameter	37.26	16.49	35.11	26.39

Table 6
Parameters of Langmuir and Freundlich adsorption isotherm and thermodynamics.

Element	Langmuir					Freundlich		
	R^2	R_L	b (L mg^{-1})	Q_{max}	ΔG/1000 (kJ/mg)	R^2	n	K_f (mg g^{-1})
Al	0.71	0.031	0.3	8.9	53.32	0.96	2.1	149
Fe	0.45	0.049	0.1	15.7	73.81	0.85	2.8	7.07
Mn	0.66	0.046	0.1	200	−137.89	0.82	2.5	1.95
SO_4^{2-}	0.55	0.062	0.002	588.2	62.80	0.92	2.3	2.4

Table 7
Calculation of SI for selected mineral phases at various pH [37].

Mineral phase	pH and saturation indices (SI)					
	3	4	6	8	10	11
Alkalinity (eq/Kg)	-3.6×10^{-2}	1.5×10^{-2}	6.4×10^{-2}	3×10^{-1}	-3×10^{-1}	3.5
$Al(OH)_3$	−0.9	3.5	2.9	1.2	−0.1	−1.5
Boehmite (AlOOH)	−0.5	7	5	3.4	2.1	0.7
Basaluminite $Al_4(OH)_{10}SO_4$	−0.8	23	17.4	6	−1.4	−10.2
Brucite $Mg(OH)_2$	−11	−9	−6.6	−2	0.6	3.6
Calcite	−11	−2.3	−1.5	1.8	3.4	4
Aragonite	−8.6	−2.5	−0.2	1.7	3.7	3.8
Diaspore (AlOOH)	−0.9	8.3	6.8	5.1	3.1	2
Dolomite $CaMg(CO_3)_2$	−6	−2.5	−1.3	4.9	6.9	8
Epsomite	−7	−4	−2	−1.8	−1.8	−1.8
$Fe(OH)_3$	5	4.4	3.7	4.6	3.2	3.1
Gibbsite $Al(OH)_3$	0.3	6.7	5.5	3.7	1.8	0.8
Geothite (FeOOH)	6	8	9.7	10.5	9.1	9
Gypsum ($CaSO_4.H_2O$)	−0.1	−0.2	−0.2	4	5	8
Jarosite H $(H_3O)Fe_3(SO_4)_2(OH)_6$	5	3.2	2.9	−3.7	−16	−20
Jurbanite ($AlOHSO_4$)	1	5	2.5	−3.6	−9.8	−12.8
Rhodochrosite ($MnCO_3$)	−8.75	−0.9	−0.4	0	0	0
Manganite MnOOH	−8.1	−5.3	−2.9	4	6	8
Pyrochroite $Mn(OH)_2$	−8	−7.1	−6.4	0.2	0.9	2.2

Table 8
Chemical composition of raw AMD before and after treatment (chemical species in mg L^{-1}).

Parameter (mg/L)	Field AMD	DWAF Guidelines	Bentonite treated AMD [22]	Magnesite treated AMD [37]	Composite treated AMD
pH	2.3	6–10	6	10.3	11.1
TDS	10237	0–1200	9872	4345.2	1145
EC	22713	0–700	16425	4635.6	2635
Na	171	0–50	316	164	223
K	18	NA	17	17	15
Mg	183	0–30	192	402	350
Ca	762	0–32	566	302	379
Al	190	0–0.9	1.1	< 0.03	< 0.03
Fe	259	0–0.1	15	<0.02	0.01
Mn	40	0–0.05	35	0.04	0.001
Cu	7.80	0–1	0.1	< 0.05	< 0.005
Zn	7.90	0–0.5	6.3	0.1	< 0.01
Pb	6.30	0–0.01	0.1	0.2	< 0.01
Co	41.30	NA	44.7	0.2	< 0.01
Ni	16.60	0–0.07	24.4	0.5	< 0.01
As	20	0.001	0.05	<0.01	<0.01
B	5	0.01	0.2	<0.01	<0.01
Cr	20	0.01	0.1	<0.01	<0.01
Mo	16	0.01	0.6	<0.01	<0.01
Se	17	0.02	0.9	<0.01	<0.01
Si	1.49	NA	5.29	5.7	0.6
SO_4^{2-}	4000	0–500	3454	1913	916

Note: DWAF stand for Department of Water Affairs and Forestry [51].

levels in the secondary residues hence justifying less conductivity in the composition of the product water.

3.3. Fourier transforms infrared spectroscopy (FTIR) analysis

The functional groups in raw and AMD-reacted composite are shown in Fig. 2.

Raw magnesite (Fig. 2, sample 1) is characterised of brucite bending corresponding to band 3702 cm^{-1}, periclase stretches corresponding to band 1500 and 950 cm^{-1} and magnesite stretching vibration corresponding to bands 1680, 1450, 850 cm^{-1}. The doublet at 1490, 1419 cm^{-1} corresponds to asymmetric stretching vibrations of carbonate. The reason for the split of this peak into a doublet could be due to the formation of new carbonates such as $CaCO_3$ and $MgCO_3$. The band at 1117 cm^{-1} correspond to symmetric stretching of carbonate, and those at 886, 795 cm^{-1} are assigned to in plane and out-of-plane bending vibrations of carbonate ion. The presence of carbonates in raw magnesite suggests the presence of Magnesite and calcite. Sharp peak at 1039 cm^{-1} belonged to the stretching of Si—O—Si bond in montmorillonite

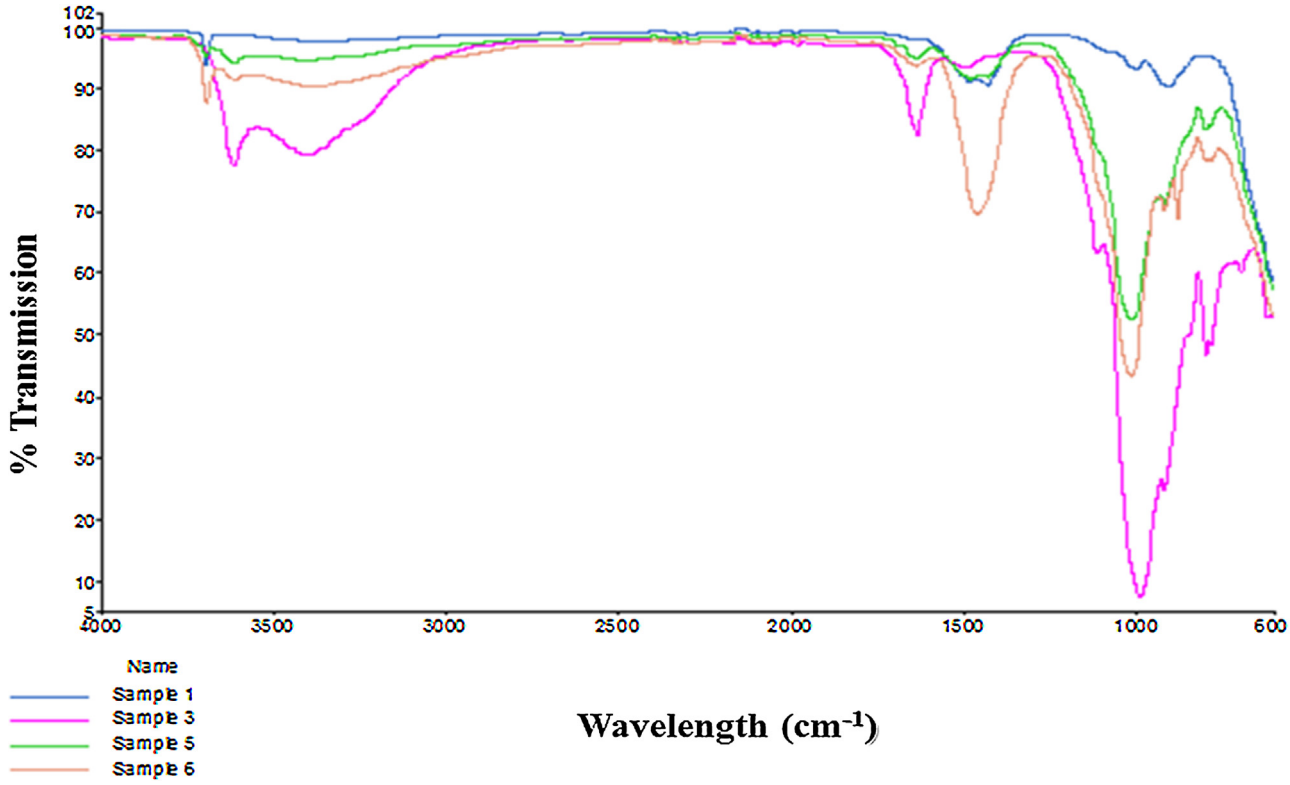

Fig. 2. FTIR spectra for magnesite (sample1), bentonite clay (sample 3), composite (sample 5) and AMD-reacted composite (sample 6).

tetrahedral sheet (Fig. 2, sample 3). Peak at 3698 cm^{-1} was due to vibration of —OH in Mg—OH, while the vibration and bending of water molecule appeared at 3450 and 1654 cm^{-1} respectively. Sharp peak at 3616 cm^{-1} was assigned to the asymmetric stretching of Al—OH—Al in the aluminosilicate sheets of pristine montmorillonite (Fig. 2, sample 5). Sharp peak at 1039 cm^{-1} is attributed to the stretching of Si-O-Si bond in montmorillonite tetrahedral sheet. Peak at 3698 cm^{-1} is attributed to vibration of–OH in Mg—OH, while the vibration and bending of OH in water molecule appeared at 3450 and 1654 cm^{-1}, respectively. Spectroscopy results also showed that there was Si—O stretching at 1023 cm^{-1} and Al—OH—Al bending at 917 cm^{-1}. OH stretching at region 3628–3260 cm^{-1} shows the presence of hydroxyl groups on the composite. This will also contribute to an increase in pH during ion exchange. Moreover, the OH band at 3623 cm^{-1} indicates the coordination of Al^{3+} with OH group. Bands in 875 cm^{-1} and 836 cm^{-1} correspond to $Fe^{2+/3+}$ and Mg^{2+}. The stretching at 1500 cm^{-1} is corresponding to CO_3 stretching for calcite and magnesite. AMD-reacted composite shows CO_3 stretches were observed to be present hence indicating the formation of carbonates (Fig. 2, sample 6). Majority of characteristic absorption bands of both bentonite clay and magnesite were also present in the composite spectra, suggesting a successful blend of the material.

3.4. Scanning electron microscope and electron dispersion X-ray (SEM-EDX)

In order to better understand the mode of interaction of AMD and magnesite–bentonite clay composite and the formation of mineral phases, SEM was utilized to depict the change in morphology of the secondary solid residues as compared with the magnesite–bentonite clay composite (Fig. 3A, C and E) and AMD-reacted magnesite–bentonite clay composite (Fig. 3B, D and F).

The surface morphology of raw composite (Fig. 3A, C and E) are showing that the composite contains leafy like structures and horny comb like structure meshed together. The structural morphology of AMD-reacted composite (Fig. 3B, D and F) are showing the leafy like structures with rod like shapes been compacted together. This indicates that contacting the composite with AMD did not alter the morphological properties of clay.

The morphologies of magnesite Fig. 4 (1), bentonite clay Fig. 4 (2), and magnesite–bentonite clay composite Fig. 4 (3) are shown in Fig. 4. SEM-EDX was utilized to semi-quantitatively identify the elemental constituent in individual minerals. Spot EDS analysis was done on selected solid residue samples (Fig. 4).

The SEM results (Fig. 4) provide important information about the morphology of magnesite, bentonite clay and the composite samples. Fig. 4 (1) shows spherical aggregates on the surface of magnesite structure. EDS revealed the presence of C, O and Mg with trace of Ca.

The SEM–EDS in Fig. 4 (2) shows that bentonite clay has sharp edges typically representing the presence of crystalline structures in raw bentonite clay. The EDS shows the presence of Al and Si at notable concentration hence indicating that they are the major species in bentonite clay structure. Fe, Mg, Ca, Na and K were observed to be presence hence indicating that these are the exchangeable cations.

The SEM–EDS in Fig. 4 (3) shows that the raw composite of irregular (heterogeneous) in shape and size, and tend to be in the form of agglomerated clusters of small particles. The EDS shows that Al, Si and Mg are the major chemical species with traces of Fe, Ca, Na and K. The presence of Na, Mg, Ca and K indicates that these are the exchangeable cations on the composite interlayers. The present results corroborate results obtained by XRF.

The morphology of AMD-reacted composite are shown in Fig. 5. SEM-EDX was utilized to semi-quantitatively identify the mineral phases resulting from the adsorption and neutralization reactions. Spot EDS analysis was done on selected solid residue samples

The SEM image (Fig. 5) shows that the particles are of the order of micrometres and have irregular shapes with sharp edges. The

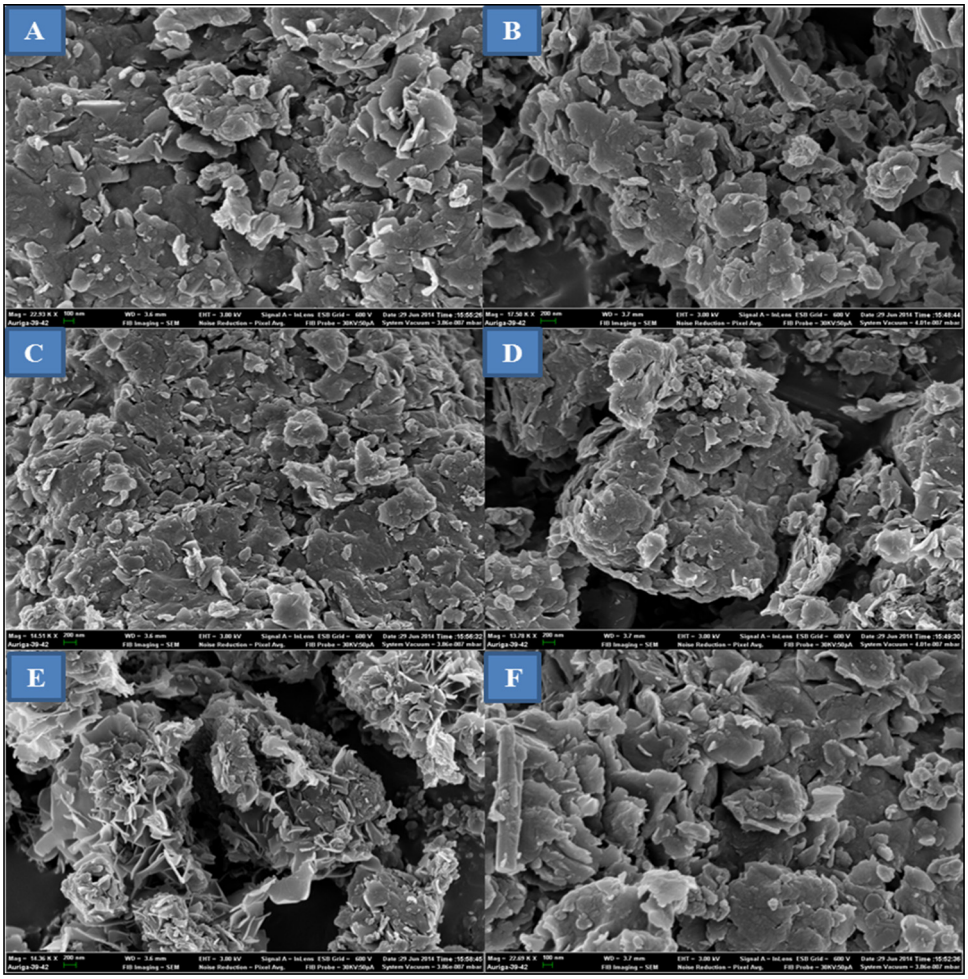

Fig. 3. Morphological properties of magnesite–bentonite clay composite (Fig. 3A, C and E) and AMD-reacted magnesite–bentonite clay composite (Fig. 3B, D and F).

agglomerates were observed to contain flowery lumps suspended on the surface of reacted composite.

Spot 1 (Fig. 5), revealed an increase in Al, Ca and Fe on the solid residues. This indicates that the species are removed from wastewater to solid residues. This confirmed by the reduction of those chemical species in the product water chemistry. The levels of Na, K and Mg were observed to have decreased. This indicates that these are the chemical species which are removed from composite interlayers when AMD is reacting with the composite since they are exchangeable cations. A decrease in Si is due to solubilisation on contact with AMD. This again indicated that bentonite clay is a sink for Fe; this was borne out by a significant reduction in levels of Fe in the product water showing that it had been adsorbed by the bentonite clay and ion exchange (release of Na, Mg, Ca and K ions) or precipitation during the dissolution of alkaline and earth alkali metals. There was a large decrease in Na on the AMD-reacted magnesite–bentonite clay composite (Fig. 5) and an increase in Na concentration in the product water (Table 8) demonstrating that it is a highly exchanged cation. Ca was observed to increase, confirming the XRD results which showed the presence of calcite in the AMD-reacted magnesite–bentonite clay composite. This indicated that calcite was being formed as AMD reacted with AMD-reacted magnesite–bentonite clay composite. Sulphur was also present in the AMD-reacted magnesite–bentonite clay composite complex indicating that the composite is a sink for sulphate from AMD, mainly as oxyhydroxysulphates or gypsum on the composite micro-surfaces. The presence of Fe, Al, Ca, Mg, C and O suggest minerals such as Fe, Al oxide, metals hydroxides, Fe carbonate, gypsum, Al and Fe oxyhydrosulphates. The PHREEQC simulation also predicted precipitation of mineral phases bearing these metal species.

Spot 2 (Fig. 5), revealed an increase in Al, Ca and Fe on the solid residues. This indicates that the species are removed from wastewater to solid residues. This confirmed by the reduction of those chemical species in the product water chemistry. The levels of Na, K and Mg were observed to have decreased. This indicates that these are the chemical species which are removed from composite interlayers when AMD is reacting with the composite since they are exchangeable cations. A decrease in Si is due to solubilisation on contact with AMD. This again indicated that bentonite clay is a sink for Fe; this was borne out by a significant reduction in levels of Fe in the product water showing that it had been adsorbed by the bentonite clay and ion exchange (release of Na, Mg, Ca and K ions) or precipitation during the dissolution of alkaline and earth alkali metals. There was a large decrease in Na on the AMD-reacted magnesite–bentonite clay composite (Fig. 5) and an increase in Na concentration in the product water (Table 8) demonstrating that it is a highly exchanged cation. Ca was observed to increase, confirming the XRD results which showed the presence of calcite in the AMD-reacted magnesite–bentonite clay composite. This indicated that calcite was being formed as AMD reacted with AMD-reacted magnesite–bentonite clay composite. Sulphur was also present in the AMD-reacted magnesite–bentonite clay composite complex indicating that the composite is a sink for sulphate from AMD, mainly as oxyhydroxysulphates or gypsum on the composite micro-surfaces. The presence of Fe, Al, Ca, Mg, C

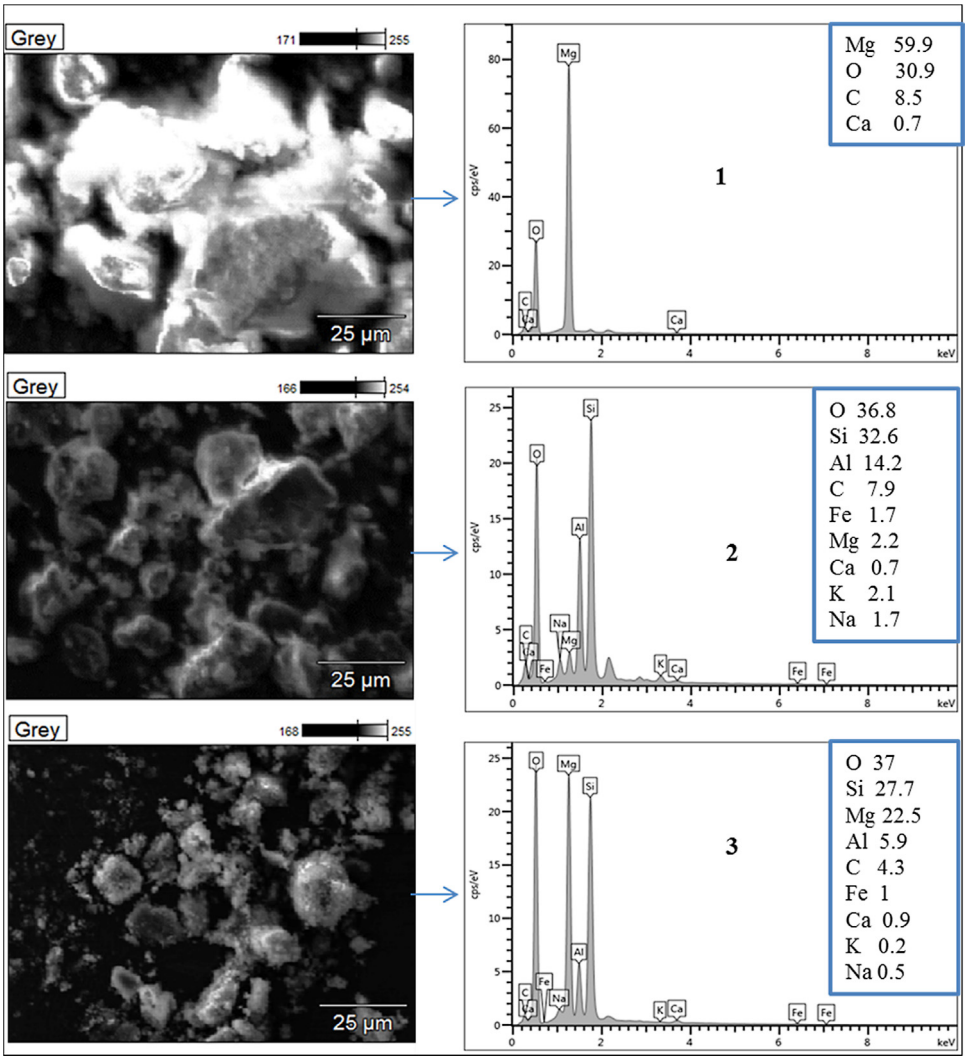

Fig. 4. SEM–EDS elemental composition of cryptocrystalline magnesite (1), bentonite clay (2) and the composite (3).

and O suggest minerals such as Fe, Al oxide, metals hydroxides, Fe carbonate, gypsum, Al and Fe oxyhydrosulphates. The PHREEQC simulation also predicted precipitation of mineral phases bearing these metal species.

Spot 3 (Fig. 5), revealed the presence of an increase in Al, Ca and Fe on the solid residues. This indicates that the species are removed from wastewater to solid residues. This confirmed by the reduction of those chemical species in the product water chemistry. The levels of Na, K and Mg were observed to have decreased. This indicates that these are the chemical species which are removed from composite interlayers when AMD is reacting with the composite since they are exchangeable cations. A decrease in Si is due to solubilisation on contact with AMD. This again indicated that bentonite clay is a sink for Fe; this was borne out by a significant reduction in levels of Fe in the product water showing that it had been adsorbed by the bentonite clay and ion exchange (release of Na, Mg, Ca and K ions) or precipitation during the dissolution of alkaline and earth alkali metals. There was a large decrease in Na on the AMD-reacted magnesite–bentonite clay composite (Fig. 5) and an increase in Na concentration in the product water (Table 8) demonstrating that it is a highly exchanged cation. Ca was observed to increase, confirming the XRD results which showed the presence of calcite in the AMD-reacted magnesite–bentonite clay composite. This indicated that calcite was being formed as AMD reacted with AMD-reacted magnesite–bentonite clay composite. Sulphur was also present in the AMD-reacted magnesite–bentonite clay composite complex indicating that the composite is a sink for sulphate from AMD, mainly as oxyhydroxysulphates or gypsum on the composite micro-surfaces. The presence of Fe, Al, Ca, Mg, C and O suggest minerals such as Fe, Al oxide, metals hydroxides, Fe carbonate, gypsum, Al and Fe oxyhydrosulphates. The PHREEQC simulation also predicted precipitation of mineral phases bearing these metal species.

3.5. Brunauer–Emmett–Teller (BET) and point of zero charge (PZC) analysis

The results for surface area for magnesite, bentonite clay, the composite and AMD-reacted composite are shown in Table 4.

Blending magnesite and bentonite clay resulted to a decrease in the surface area of the composite as compared to bentonite clay alone. The synthesized composite was determined to contain a surface area of 18.36 which decreased to 16.17 m^2/g after contacting the AMD hence indicating that the vacant surfaces on composite surfaces are occupied with specs of precipitating mineral phases which would block the pores of the composite reducing its surface area (Table 4). This indicates the possible adsorption and deposition of materials to clay surfaces. The pH_{pzc} gives an insight on the type

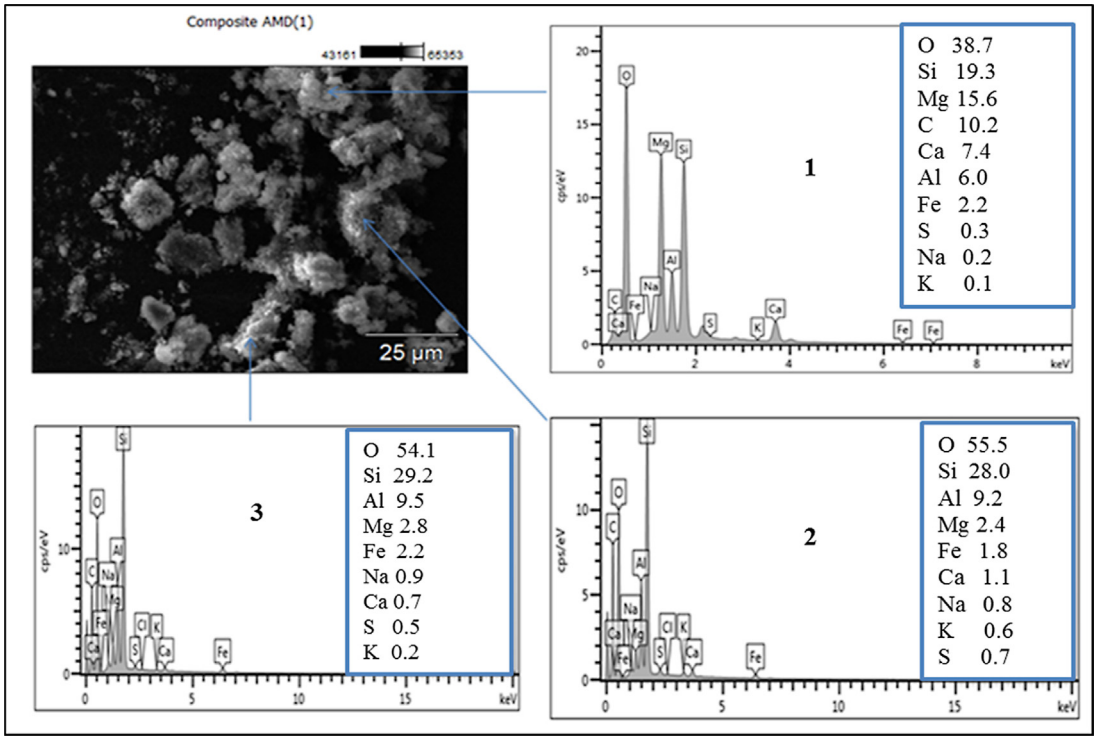

Fig. 5. SEM–EDS elemental composition of AMD-reacted magnesite–bentonite clay composite.

of chemical species that are more likely to be removed from aqueous solution during the reaction. In the present study, the point of zero charge were observed to be 10 for magnesite, 8 for bentonite clay, 10 for the composite and 10 for the reacted composite. When pH_{pzc} is greater than the supernatant pH, the adsorbent will adsorb anions. When the pH of the supernatant is above the pH_{pzc} the adsorbent will adsorb cations from the solution. A study by [46] pointed out that aluminium and iron oxides have high pH_{PZC} values (≈8). The high pH_{PZC} of bentonite clay is due to the presence of aluminium and iron oxides or hydroxides in the clay matrix. The pH_{pzc} value of a material is a reflection of the individual pH_{pzc} values of the components present. Clay and oxide contents increase the pH_{pzc} of the material [47]. Chemical interaction could have occurred through multidentate ligands with the surface hydroxyl groups hence leading to inner and outer layer complexes [48].

3.6. Inorganic contaminants removal: batch experiments

3.6.1. Effects of magnesite to bentonite ratios

The results for inorganic contaminants attenuation as a function of magnesite to bentonite clay ratios are shown in Fig. 6.

Variation of the removal efficiencies in neutralization and removal of metals species and sulphate by the composite with different contents of cryptocrystalline magnesite are shown in Fig. 6. It is clear that wt% of cryptocrystalline magnesite, in the composite is an important factor affecting the neutralization and removal of metals and sulphate ions from aqueous solution, especially in highly acidic environment. Fig. 6 shows that as the ratio of magnesite to bentonite increases, there was a proportional increase in pH. The pH was observed to increase from ≈10.2 to ≈12.3. This was attributed to the dissolution of magnesite and partly to the release

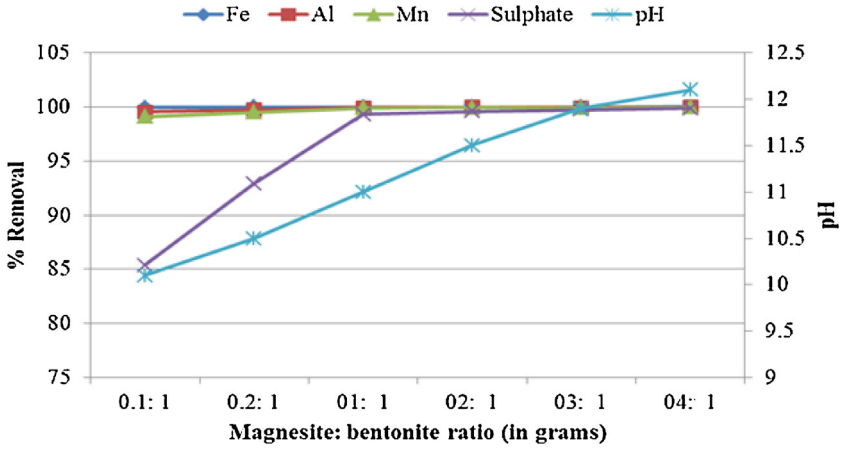

Fig. 6. Variation in% removal of Fe^{3+}, Al^{3+}, Mn^{2+} and sulphate as a function of solid to solid ratios (Conditions: pH < 3, 2000 mg/L Fe^{3+}, 200 mg/L Al^{3+}, 100 mg/L Mn^{2+}, 6250 mg/L SO_4^{2-}, 60 mins shaking time, 100 mL SAMD solution, 32 µm particle size, 250 rpm shaking speed, 26 °C temperature).

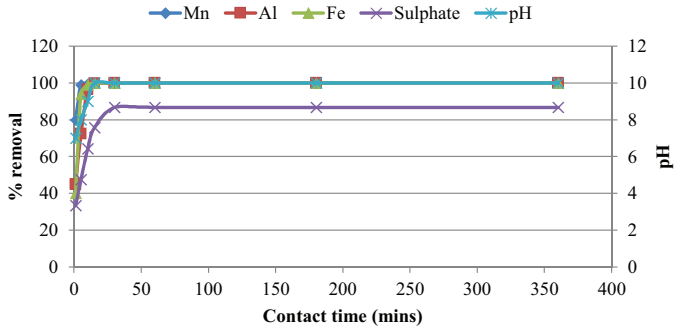

Fig. 7. Variation of Al, Fe, Mn and SO_4^{2-} with agitation time and variation of pH with agitation time (Conditions: pH < 3, 2000 mg/L Fe^{3+}, 200 mg/L Al^{3+}, 100 mg/L Mn^{2+}, 6250 mg/L SO_4^{2-}, 1 g composite, 100 mL SAMD solution, 1; 100 S/L ratios, 32 μm particle size, 250 rpm shaking speed, 26 °C ambient temperature).

of base cations from the bentonite clay matrices as shown in the reactions below.

$$MgO + H_2O \rightarrow Mg^{2+} + 2OH^- \quad (17)$$

$$CaO + H_2O \rightarrow Ca^{2+} + 2OH^- \quad (18)$$

$$Na_2O + H_2O \rightarrow 2Na^+ + 2OH^- \quad (19)$$

$$K_2O + H_2O \rightarrow 2K^+ + 2OH^- \quad (20)$$

Removal of sulphate was observed to increase with an increase in the magnesite to bentonite ratio. Attenuation of the major metal species concentrations, Al, Mn and Al remained above 99% since the pH was highly alkaline for their precipitation. At 1:1 magnesite to bentonite all the chemical species removal was above 98% and the higher ratios seemed to have no significant difference in the removal capacity. Hence a 1:1 ratio was taken as the optimum for the fabrication of the composite.

3.6.2. Effect of equilibration time

Results of metals species and sulphate removal in SAMD as a function of contact time are shown in Fig. 7.

An increase in pH was observed with increases in contact time. Metal removal also increased with increased contact time. An increase in pH from 6 to 10 and metal concentration attenuations were observed to be high within the first 20 min of interaction but stabilizes thereafter. An increase in pH was attributed to dissolution of magnesite, alkali and alkaline earth metal oxides from the composite during the interaction with AMD leading to an increase in alkalinity. An increase in pH also leads to precipitation of metal species from AMD. On precipitation the metal hydroxides incorporate sulphate to form various oxyhydroxysulphates and also adsorb sulphate. The composite also exchanged Al^{3+}, Fe^{3+}, and Mn^{2+} with cations such as Na^+, Mg^{2+} and Ca^{2+} in their matrices, the exchanged highly charged cations could also adsorb sulphates as the counter ions. The composite showed good efficiencies in the treatment of AMD since it remove chemical species from contaminated water in a single step as compared to two-step traditional treatment methods. This study also showed good removal efficiencies of chemical species (≈100% Al^{3+}, Fe^{3+}, and Mn^{2+} and >50% SO_4^{2-}) as compared to a study conducted by Nkonyane et al. [49] who reported that 120 min of contact time is efficient in raising the pH to 7.5 and remove metals except for Mn when using a combination of bentonite clay and limestone. The present study achieved maximum removal within the short contact time of 20 min and raised the pH to >10 which is suitable for removal of all metal species. Therefore, 30 min was taken as the optimum agitation time and it will be used as optimum time and applied in subsequent experiments.

3.6.3. Adsorption kinetics and mechanism

The effect of contact time on removal of chemical species from aqueous solution was evaluated using different kinetic models to reveal the nature of the adsorption process and rate limiting processes. Different kinetic model parameters for adsorption of Mn, Al, Fe and sulphate on the composite are shown in Table 5.

The experimental data was fitted by using the pseudo-first-order kinetic model by plotting $\ln(q_e - q_t)$ vs. t, and the results are shown in Table 5 and Fig. 8. The pseudo-first-order was applied and it was found to fairly converge with the experimental data. Moreover, the calculated amounts of Mn, Al, Fe and sulphate ions adsorbed by the composite [$q_{e,calc}$ (mgg^{-1})] were less than the experimental values [$q_{e,exp}$ (mgg^{-1})] (Table 5). The finding indicated that the Lagergren pseudo-first-order kinetic model is inappropriate to describe the adsorption of Mn, Al, Fe and sulphate ions from aqueous system by the composite.

An application of the pseudo-second-order rate equation for adsorption of chemical species to the composite matrices portrayed a good fit with experimental data (Fig. 8–10 and Table 5). The obtained results confirm that pseudo-second-order model is the most suitable kinetic model to describe adsorption of Mn, Al, Fe and sulphate by the composite from aqueous system. Moreover, this also confirms that the adsorption mechanism of the metals species from aqueous solution is chemisorption. Note the theoretical adsorption capacity is close to the experimental adsorption capacity further confirming that this model describes the adsorp-

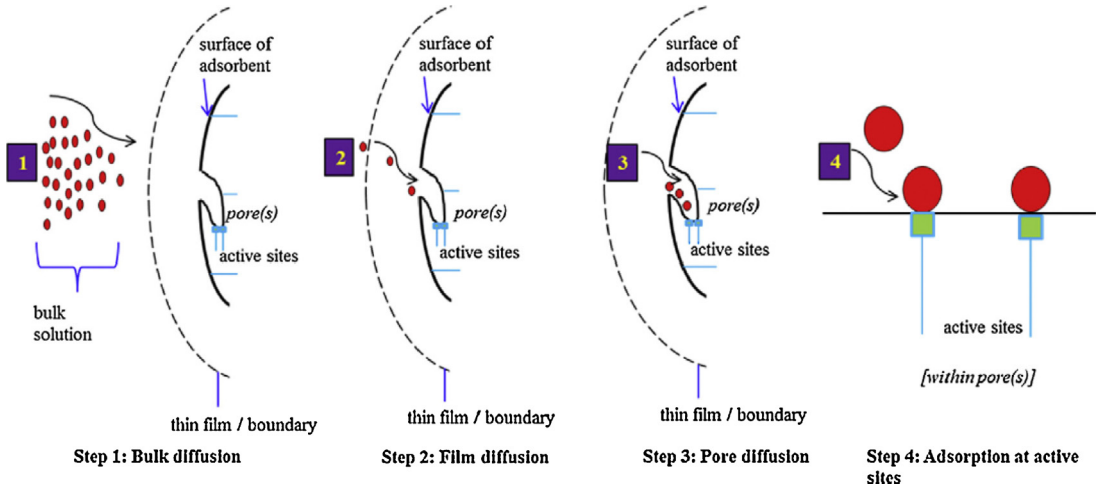

Fig. 8. Proposed diagram for the transportation of solute to adsorbent (not to scale).

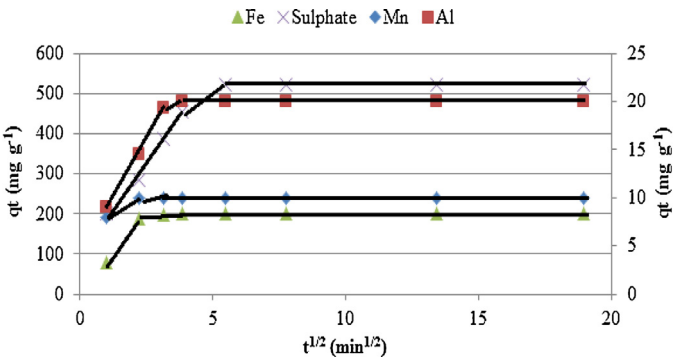

Fig. 9. Intraparticle diffusion plots of Mn, Al, Fe and sulphate ions adsorbed on the composite.

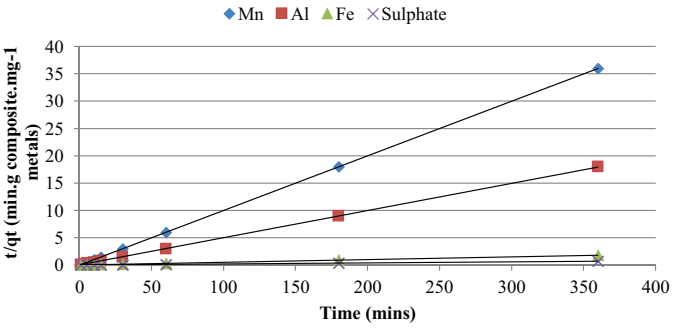

Fig. 10. Pseudo-second-order plots of Mn, Al, Fe and sulphate ions adsorbed on the composite.

tion data (Table 5 and Fig. 9). Given the multi-linear nature of the plot for metal species sorption on the composite, it is proposed that sorption occurred in three phases. The initial steep phase represented surface diffusion, the second less steep phase represented a gradual sorption of metal species where intra-particle diffusion within the pores is rate-limiting, and the third phase where equilibrium had been achieved. Since the plot did not pass through the origin, intra-particle diffusion was not the only rate-limiting step. There were three processes controlling metals species sorption rate but only one predominates at any particular time phase. The C_i (mg g^{-1}) values indicate the thickness of the boundary layer which was observed to be very small for these soils; and these low C values suggested that surface diffusion plays fewer roles as the rate-limiting step in the overall sorption process. The results also showed that the Intraparticle diffusion model by Webber Morris was not applicable for the present process due to lower correlation coefficients. To explain the mechanism of intra-particle diffusion, the Weber Morris model is used to illustrate the concept. Interaction of solute with the adsorbent can be defined by four major steps: Bulk diffusion, film diffusion, pore diffusion and adsorption at active sites (Fig. 7) [50]

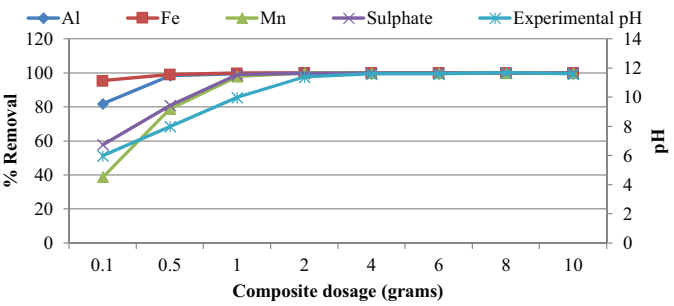

Fig. 11. Variation of pH, Al, Fe, Mn and sulphate concentration with adsorbent dosage (conditions: pH < 3, 2000 mg/L Fe^{3+}, 200 mg/L Al^{3+}, 100 mg/L Mn^{2+}, 6250 mg/L SO_4^{2-}, 100 mL solution, 250 rpm shaking speed, <32 μm particle size, 30 min reaction, 26 °C temperature).

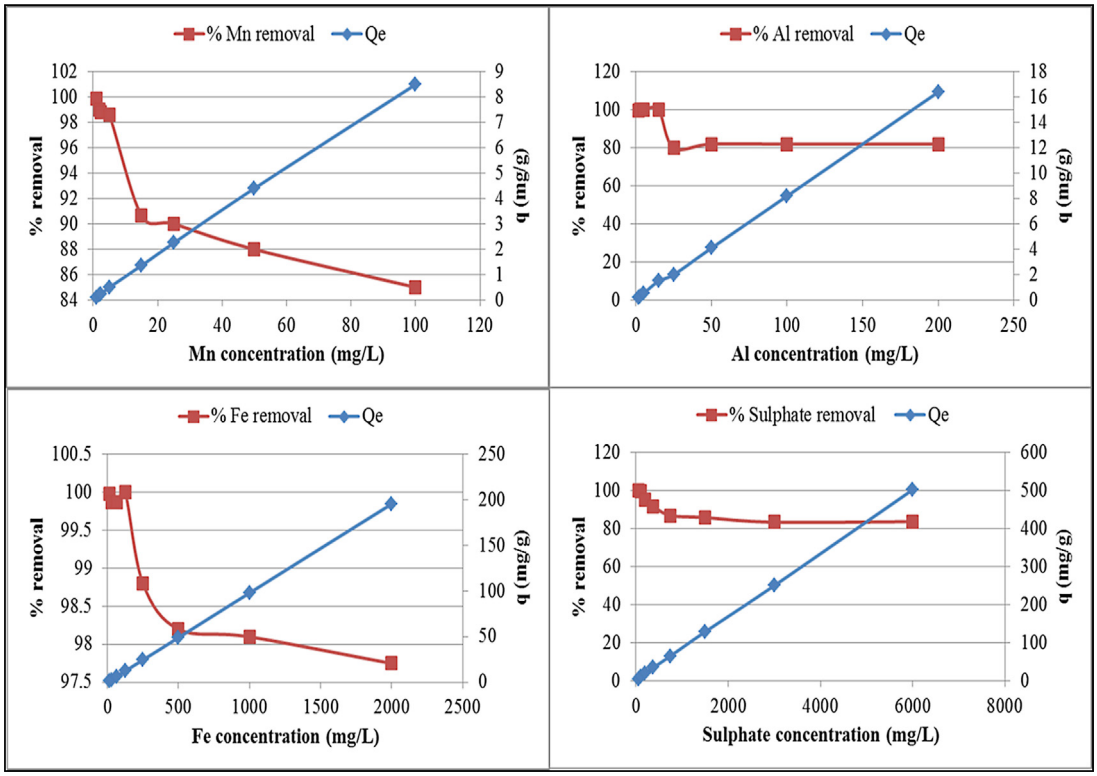

Fig. 12. Variation in% removal and adsorption capacity of Al^{3+}, Mn^{2+} and $Fe^{3+/2+}$ as a function of ion concentration (pH < 3, 30 mins of shaking, < 32 μm particle size, 1 g composite, 100 mL, 1:100 S/L ratios, 250 rpm shaking speed, and 26 ° C ambient temperature).

The plot of $t^{0.5}$ and q_t (mg g^{-1}) by Webber Morris model indicated that there are more than one rate limiting steps that are involved when an adsorbate is being removed from aqueous solution. The first step which a very steep slope which is by film diffusion (2), the second step which is slightly steep represent pore diffusion (3) and the final step of linearity which indicate that the reaction has approached the equilibrium phase. The linear plots did not pass through the origin hence indicating that intra-particle diffusion is not the only step governing the chemical reaction. The lower K_{id}(mg g^{-1} min$^{-1/2}$) indicate that the adsorption process is taking place at a very fast rate with high adsorption capacity as represented by high C_i(mg g^{-1}) (Table 5) which is pretty much close to the experimental value.

The plot for adsorption of Mn, Al, Fe and sulphate on the composite using pseudo-second-order is shown in Fig. 10.

3.6.4. Effects of composite dosage

The results of neutralization and attenuation of inorganic contaminants from synthetic AMD as a function of the composite dosage are shown in Fig. 11.

Fig. 11 shows that there was an increase in pH with an increase in composite dosage. Cations and anions in the supernatant solution were also observed to decrease with an increase in dosage. The increase in pH was attributed to dissolution of magnesite, alkali and alkaline earth metal oxides from the composite during the interaction with AMD, hence leading to an increase in pH. The XRF and XRD results also indicated the presence of these oxides and carbonates in the matrices of the feedstock. An increase in pH also led to precipitation of metal species from AMD. On precipitation the metal hydroxides incorporate sulphates to form various oxyhydroxysulphates and also adsorb sulphates. The adsorption data could further point to chemical adsorption probably due to interaction with the $[Al(H_2O)_6]^{3+}$ and $[Fe(H_2O)_6]^{3+}$ incorporated to the interlayers and hydroxyl groups on the clay surfaces. When this pH is reached, small particles of the metal hydroxide are formed (Eq. (21)). For example sulphate could interact with those species as follows [Eqs. (22)– (23)].

$$M^{n+} + nOH^- \rightarrow M(OH)_n \downarrow \quad (21)$$

$$Al(H_2O)_3(OH)_3 + SO_4^{2-} \rightarrow Al(H_2O)_3(OH)(SO_4) + 2OH^- \quad (22)$$

$$Fe(H_2O)_3(OH)_3 + SO_4^{2-} \rightarrow Fe(H_2O)_3(OH)(SO_4) + 2OH^- \quad (23)$$

The composite may also exchange Al^{3+}, Fe^{3+}, and Mn^{2+} with cations such as Na^+, Mg^{2+} and Ca^{2+} in their matrices (Table 2). The exchanged high charge cations could also adsorb sulphates as the counter ions. As composite dosage increased, the pH increased. Moreover, the composite presented more sites for ion-exchange and adsorption of chemical species in aqueous solution. As the dosage increased, more surface sites for exchange of low density cations with high density cations from AMD become available. The composite is effective for AMD treatment since it combines ion-exchange of (Mg, Ca, Na and K), adsorption, co-precipitation and precipitation of metal species from AMD as the pH increase due to dissolution of alkaline materials hence leading to much cleaner effluents. At 1 g adsorbent dosage the attenuation capacity of the major metal species concentrations was >95%. Consequently, 1 g was taken as the optimum dosage for subsequent experiments under these conditions. The optimum dosage (10 g/L) indicated by this work compares favourably with other remediation agents such as limestone (10 g/L), dolomite (40 g/L), limestone bentonite blend (10 g/L) and fly ash (500 g/L) [35,49,16]. Moreover, the treatment efficiency of this technology is high as compared to the other technologies since it can neutralize and remove metals and sulphate to within DWS drinking water quality guidelines. South Africa has large reserves of both bentonite [5] and magnesite [34], and thus, the economic viability of this technology is high.

3.6.5. Effects of chemical species concentration

The results for chemical species attenuation as a function of concentration are shown in Fig. 12.

At the initial concentration evaluated the composite exhibited ≈80–100 for Al, ≈97–100 for Fe, and ≈84–100 for Mn removal efficiency. Greater than 80% sulphate removal efficiency was observed at the evaluated concentration ranges. The pH remained above 10 in all concentration gradients meaning that 30 min of agitation and 1 g of the composite would be adequate for neutralization and removal of contaminates from AMD under these conditions. At low concentration of metal species, more surfaces are available for adsorption and at high concentration more surfaces are occupied by pollutants. At low concentration, there is less acidity to be neutralised so the pH remain alkaline (>10). Removal of Al and Fe may be due to ion exchange of base cations (Mg, Ca, Na and K) from the composite interlayers, dissolution of magnesite leading to precipitation and co-precipitation of metal species with an increase in pH. The presence of exchangeable base metals was shown by CEC, SEM–EDS and XRF studies (Table 2 and 6). Dissolution of calcite, periclase and magnesite as shown by XRD contribute to an increase in pH that will precipitate metals as hydroxide and oxyhydrosulphates as shown by SEM–EDS point analysis (Fig. 5).

3.6.6. Adsorption isotherms and thermodynamics

The relationship between the amount of ions adsorbed and the ion concentration remaining in solution is described by an isotherm. The two most common isotherm models for describing this type of system are the Langmuir and Freundlich adsorption isotherms. These models describe adsorption processes on a homogenous (monolayer) or heterogeneous (multilayer) surface, respectively. The parameters of Langmuir and Freundlich adsorption isotherms are shown in Table 6.

The results showed better fit to Freundlich adsorption isotherm than Langmuir adsorption isotherm hence confirming multilayer adsorption. Q_{max} and b were determined from the slope and intercept of the plot and were found to be 8.9, 15.7, 200, 588.2 mg/g and 0.3, 0.1, 0.1, 0.002 L/mg for Mn, Al, Fe and sulphate, respectively. According to Sparks (2003), R_L values between 0 and 1 indicate favourable adsorption. The R_L were found to range from 0.031 to 0.062 hence showing that it was favourable. K_f and n were calculated from the slopes of the Freundlich plots. The constants were found to be K_f = 149, 7.07, 1.95, 2.4 and n = 2.1, 2.8, 2.5, 2.3 for Mn, Al, Fe and sulphate, respectively. According to Langmuir (1997), n values between 1 and 10 represent beneficial adsorption. This showed that adsorption of ions from aqueous solution by the composite was favourable. Gibbs free energy model predicted that the reaction is spontaneous in nature for Al, Fe and sulphate except for Mn.

3.7. Variation of pH with an increase in Fe^{3+} concentration

The variation of pH profile with varying concentration of Fe^{3+} as representative of the inorganic contaminants in the SAMD is shown in Fig. 13.

As the metal concentration increases, the initial pH was gradually decreasing, this may be attributed to hydrolysis of metal cations with the release of H^+ cations.

$$Fe^{3+} + H_2O \rightarrow Fe(OH)_{3(s)} + H^+ \quad (24)$$

$$Al^{3+} + H_2O \rightarrow Al(OH)_{3(s)} + H^+ \quad (25)$$

$$Mn^{2+} + H_2O \rightarrow Mn(OH)_{2(s)} + H^+ \quad (26)$$

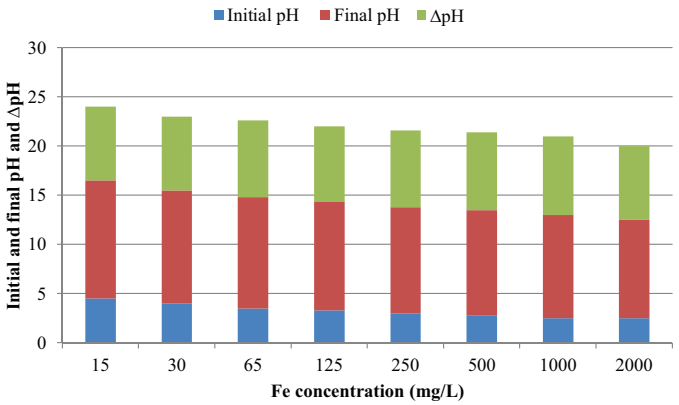

Fig. 13. Variation of pH gradient with varying sulphate concentrations.

As shown in Fig. 13, drastic increases in final pH were observed at varying Fe concentrations. Increases in pH were attributed to dissolution of calcite, periclase and magnesite, and release of base metal species from the clay matrices to aqueous solution. Adsorption of sulphate onto clay matrices with release of hydroxyl groups may also have contributed to increases in pH of the aqueous solutions.

4. Calculation of saturation indices (SI) for various mineral phases

The results for calculation of mineral precipitation at various pH values during treatment of simulated AMD with magnesite–bentonite clay composite are presented in Table 7.

As shown in Table 7, Fe could precipitate as hydroxides at pH > 3. Al could precipitate as hydroxides at pH > 4. Mn could precipitates as hydroxide at pH > 10 and rhodochrosite at pH > 8. Sulphate-bearing minerals could precipitates at pH 6–8 (basaluminite), pH > 8 (gypsum), pH 6 (jarosite and jurbanite). PHREEQC predicted mineral phases to precipitate as metal hydroxides, hydroxysulphates and oxyhydroxysulphates. However, sulphates were removed from solution together with Al, Fe and Ca. This corroborate the SEM–EDX and XRF detected Al, Fe, Mn and S rich mineral phases were deposited to solid residues. This indicates that the Al, Fe, Mn and S rich mineral phases were too amorphous to be detected by XRD or the concentration was below the detection limits. To be particular, the presence of Mn, Fe, Al, Ca, Mg, C and O suggest precipitation of minerals such as Mn, Fe, Al oxide, metals hydroxides, Mn and Fe carbonate, gypsum, Al and Fe oxyhydrosulphates, this was validated by PHREEQC geochemical model and SEM–EDS.

5. Treatment of field AMD at optimized conditions

The results of AMD treatment with bentonite clay, magnesite and the composite are shown in Table 8.

In field AMD the major ions are Ca, Mg, Na, Al, Fe and sulphate. After treatment, the resultant water had an increased pH with reduced metal species and sulphate concentrations. The composite treatment yielded water to within the DWAF Water Quality Guidelines. Bentonite showed insignificant increase in pH and a slight reduction in metal species. This showed that the treatment is effective for wastewater with low metal concentrations and as such it can be used as a polishing process. Contact of cryptocrystalline magnesite at optimised conditions produced water conforming to the DWAF Water Quality Guidelines except for pH, EC, TDS, Mg and sulphate. A combination of magnesite and bentonite clay treatment increased the pH of the solution significantly and yielded water conforming to DWAS Guidelines. The pH was >11, major metals removal was >99%, oxyanions of As, B, Cr, Mo, Se and sulphate were also removed significantly (>90%) while alkali and alkaline earth metals were also moderately removed (>60%) hence indicating the superiority of the composite in the acid effluent treatment.

6. Conclusion

The vibratory ball mill was successfully used for the synthesis of the cryptocrystalline magnesite and bentonite clay composite. The pronounced efficiencies in neutralization and attenuation of inorganic contaminants from AMD were observed to be superior as compared to bentonite clay and cryptocrystalline magnesite used individually. It was observed that the best conditions for synthesis of the composite are 1:1 wt%. Milling improved the physicochemical properties of the composite hence making the composite an excellent material for neutralization and attenuation of inorganic contaminants simultaneously. This makes the present study to conclude that the magnesite–bentonite composite has the capacity to neutralize AMD and remove potentially toxic chemical species. Optimization experiments revealed that 20 min of equilibration and 1 g of composite dosage were the optimum conditions under these laboratory conditions for treatment of AMD at 1:100 S/L ratios. Four processes were observed to govern the removal of inorganic contaminants from AMD using the composite, namely, (1) adsorption, (2) ion-exchange (3) precipitation and (4) co-precipitation. The adsorption process fitted to pseudo-second-order kinetics rather than pseudo-first-order kinetics, confirming that the step governing chemical reaction is chemisorption. In adsorption modelling the data conformed better to the Freundlich adsorption isotherm than Langmuir adsorption isotherm hence confirming multilayer adsorption. An increase in the levels of base cations in the product water as shown by ICP-MS and a decrease in the secondary residue as shown by XRF, and SEM–EDS indicates that ion exchange was one of the mechanisms that were taking place during the removal of metal species from contaminated water bodies. PHREEQC geochemical model, revealed that Fe, Al, Mn, and Ca formed sulphate-bearing minerals. SEM–EDS, disclosed that the presence of Fe, Al, Ca, Mg, C and O suggest minerals such as Fe, Al oxide, metals hydroxides, Fe carbonate, gypsum, Al and Fe oxyhydrosulphates are formed as precipitates or co-precipitates. From modelling simulations, the formation of these phases follow a selective precipitation sequence with Fe^{3+} at pH > 6, Al^{3+} at pH > 6, Fe^{2+} at pH > 8, Mn^{2+}, Ca^{2+} and Mg^{2+} at pH > 10. The composite proved to be effective for treatment of AMD as compared to traditional wastewater treatment methods such as limestone, magnesite, clays, lime and bentonite blend. It also produced water of usable standard for industrial and agricultural purposes. This study showed that magnesite and bentonite clay composite can be an efficient and effective technology for treatment of AMD.

Acknowledgements

The authors wish to express their sincere gratitude to the Council for Scientific and Industrial Research (CSIR), Environmental Remediation and Water Pollution Chemistry Research Group, University of Venda Directorate, Department of Ecology and Resource Management, ESKOM-TESP, SASOL-Inzalo, and DST-NRF for supporting this project financially.

References

[1] G.S. Simate, S. Ndlovu, Acid mine drainage: challenges and opportunities, J. Environ. Chem. Eng. 2 (2014) 1785–1803.
[2] D.W. Blowes, C.J. Ptacek, J.L. Jambor, C.G. Weisener, D. Paktunc, W.D. Gould, D.B. Johnson, 11.5—the geochemistry of acid mine drainage, in: H.D.H.K. Turekian (Ed.), Treatise on Geochemistry, second edition, Elsevier, Oxford, 2014, pp. 131–190.

[3] H. Tutu, T.S. McCarthy, E. Cukrowska, The chemical characteristics of acid mine drainage with particular reference to sources, distribution and remediation: the Witwatersrand Basin, South Africa as a case study, Appl. Geochem. 23 (2008) 3666–3684.
[4] N.P. Cheremisinoff, Groundwater Remediation and Treatment Technologies, Elsevier Science, 1998.
[5] W.M. Gitari, Attenuation of metal species in acidic solutions using bentonite clay: implications for acid mine drainage remediation, Toxicol. Environ. Chem. (2014).
[6] K.B. Hallberg, New perspectives in acid mine drainage microbiology, Hydrometallurgy 104 (2010) 448–453.
[7] A.S. Sheoran, V. Sheoran, R.P. Choudhary, Geochemistry of acid mine drainage: a review, Perspect. Environ. Res. (2011) 217–243.
[8] R.W. Gaikwad, Review and research needs of active treatment of acid mine drainage by ion exchange, Electron. J. Environ. Agric. Food Chem. 9 (2010) 1343–1350.
[9] M. Zhang, Adsorption study of Pb(II), Cu(II) and Zn(II) from simulated acid mine drainage using dairy manure compost, Chem. Eng. J. 172 (2011) 361–368.
[10] E. Macingova, A. Luptakova, Recovery of metals from acid mine drainage by selective sequential precipitation processes, 11th International Multidisciplinary Scientific Geoconference and EXPO—Modern Management of Mine Producing, Geology and Environmental Protection, SGEM 2011 (2011) 573–578.
[11] F.I. Ramírez-Paredes, T. Manzano-Muñoz, J.C. Garcia-Prieto, G.G. Zhadan, V.L. Shnyrov, J.F. Kennedy, M.G. Roig, Biosorption of heavy metals from acid mine drainage onto biopolymers (chitin and α (1,3) β-D-glucan) from industrial biowaste exhausted brewerαs yeasts (*Saccharomyces cerevisiae* L.), Biotechnol. Bioprocess Eng. 16 (2011) 1262–1272.
[12] J.P. Maree, P. Du Plessis, Neutralization of acid mine water with calcium carbonate, Water Sci. Technol. 29 (1994) 285–296.
[13] C. Cruz Viggi, F. Pagnanelli, A. Cibati, D. Uccelletti, C. Palleschi, L. Toro, Biotreatment and bioassessment of heavy metal removal by sulphate reducing bacteria in fixed bed reactors, Water Res. 44 (2010) 151–158.
[14] T.T. Wei, Y. Yu, Z.Q. Hu, Y.B. Cao, Y. Gao, Y.Q. Yang, X.J. Wang, P.J. Wang, Research progress of acid mine drainage treatment technology in China, Appl. Mech. Mater. (2013) 214–220.
[15] V. Bologo, J.P. Maree, F. Carlsson, Application of magnesium hydroxide and barium hydroxide for the removal of metals and sulphate from mine water, Water SA 38 (2012) 23–28.
[16] J.P. Maree, M. Mujuru, V. Bologo, N. Daniels, D. Mpholoane, Neutralisation treatment of AMD at affordable cost, Water SA 39 (2013) 245–250.
[17] V. Masindi, M.W. Gitari, H. Tutu, M. De Beer, Application of magnesite–bentonite clay composite as an alternative technology for removal of arsenic from industrial effluents, Toxicol. Environ. Chem. 96 (2014) 1435–1451.
[18] V. Masindi, W.M. Gitari, T. Ngulube, Defluoridation of drinking water using Al3+ -modified bentonite clay: optimization of fluoride adsorption conditions, Toxicol. Environ. Chem. 96 (2014) 1294–1309.
[19] V. Masindi, M.W. Gitari, H. Tutu, M. De Beer, Synthesis of a porous magnesite-bentonite clay composite and its application for neutralisation and attenuation of inorganic contaminants in acidic and metalliferous mine drainage, in: ICEN 2015 Conference Proceeding on Environment, Malaysi, Penang, 2015, pp. 69–77.
[20] V. Masindi, M.W. Gitari, H. Tutu, M. Debeer, Removal of boron from aqueous solution using magnesite and bentonite clay composite, Desalin. Water Treat. (2015) 1–11.
[21] V. Masindi, W.M. Gitari, Simultaneous removal of metal species from acidic aqueous solutions using cryptocrystalline magnesite/bentonite clay composite: an experimental and modelling approach, J. Clean. Prod. (2015).
[22] V. Masindi, W.M. Gitari, H. Tutu, M. De Beer, Efficiency of ball milled South African bentonite clay for remediation of acid mine drainage, Water Process Eng. (2015).
[23] Y. Zhao, L.-y. Zhang, F. Ni, B. Xi, X. Xia, X. Peng, Z. Luan, Evaluation of a novel composite inorganic coagulant prepared by red mud for phosphate removal, Desalination 273 (2011) 414–420.
[24] S.S. Gupta, K.G. Bhattacharyya, Removal of Cd(II) from aqueous solution by kaolinite, montmorillonite and their poly(oxo zirconium) and tetrabutylammonium derivatives, J. Hazard. Mater. 128 (2006) 247–257.
[25] K.G. Bhattacharyya, S.S. Gupta, Removal of Cu(II) by natural and acid-activated clays: an insight of adsorption isotherm, kinetic and thermodynamics, Desalination 272 (2011) 66–75.
[26] A.B. Đukić, K.R. Kumrić, N.S. Vukelić, M.S. Dimitrijević, Z.D. Baščarević, S.V. Kurko, L.L. Matović, Simultaneous removal of Pb^{2+}, Cu^{2+}, Zn^{2+} and Cd^{2+} from highly acidic solutions using mechanochemically synthesized montmorillonite-kaolinite/TiO2 composite, Appl. Clay Sci. 103 (2015) 20–27.
[27] G. Zhuang, Z. Zhang, J. Guo, L. Liao, J. Zhao, A new ball milling method to produce organo-montmorillonite from anionic and nonionic surfactants, Appl. Clay Sci. 104 (2015) 18–26.
[28] K. W. Kim, H. Kim, M. Lee, S. Kim Shin, Mechanochemical activation on the preparation of β-eucryptite from powder mixture of pyrophyllite, gibbsite and lithium carbonate, Mater. Trans. 54 (2013) 380–383.
[29] V. Masindi, W. Gitari Mugera, The potential of ball-milled South African bentonite clay for attenuation of heavy metals from acidic wastewaters: Simultaneous sorption of Co^{2+}, Cu^{2+}, Ni^{2+}, Pb^{2+}, and Zn^{2+} ions, J. Environ. Chem. Eng. 3 (2015) 2416–2425.
[30] V. Masindi, M.W. Gitari, H. Tutu, M. DeBeer, Efficiency of ball milled South African bentonite clay for remediation of acid mine drainage, J. Water Process Eng. 8 (2015) 227–240.
[31] A. Djukić, U. Jovanović, T. Tuvić, V. Andrić, J. Grbović Novaković, N. Ivanović, L. Matović, The potential of ball-milled Serbian natural clay for removal of heavy metal contaminants from wastewaters: simultaneous sorption of Ni, Cr, Cd and Pb ions, Ceram. Int. 39 (2013) 7173–7178.
[32] K.G. Bhattacharyya, S.S. Gupta, Adsorption of a few heavy metals on natural and modified kaolinite and montmorillonite: a review, Adv. Colloid Interface Sci. 140 (2008) 114–131.
[33] S.S. Gupta, K.G. Bhattacharyya, Kinetics of adsorption of metal ions on inorganic materials: a review, Adv. Colloid Interface Sci. 162 (2011) 39–58.
[34] V. Masindi, M.W. Gitari, H. Tutu, M. De Beer, Application of magnesite–bentonite clay composite as an alternative technology for removal of arsenic from industrial effluents, Toxicol. Environ. Chem. (2014) 1–17.
[35] M. Gitari, L. Petrik, O. Etchebers, D. Key, E. Iwuoha, C. Okujeni, Treatment of acid mine drainage with fly ash: Removal of major contaminants and trace elements, J. Environ. Sci. Health Part A Toxic/Hazard. Subst. Environ. Eng. 41 (2006) 1729–1747.
[36] V. Masindi, M.W. Gitari, H. Tutu, M. De Beer, Neutralization and attenuation of metal species in acid mine drainage and mine leachates using magnesite: a batch experimental approach, in: Sui, Sun, Wang (Eds.), An Interdisciplinary Response to Mine Water Challenges, China University of Mining and Technology Press, Xuzhou, 2014, pp. 640–644.
[37] V. Masindi, W. Gitari, H. Tutu, M. DeBeer, Passive remediation of acid mine drainage using cryptocrystalline magnesite: a batch experimental and geochemical modelling approach, Water SA 41 (2015) 677–682.
[38] S.S. Potgieter-Vermaak, J.H. Potgieter, P. Monama, R. Van Grieken, Comparison of limestone, dolomite and fly ash as pre-treatment agents for acid mine drainage, Miner. Eng. 19 (2006) 454–462.
[39] T. Falayi, F. Ntuli, Removal of heavy metals and neutralisation of acid mine drainage with un-activated attapulgite, J. Ind. Eng. Chem. 20 (2014) 1285–1292.
[40] C. J. Shou, F. Jiang, M. Wang, Q. Xu Qiu, Fabrication of Fe_3O_4/MgAl-layered double hydroxide magnetic composites for the effective decontamination of Co(II) from synthetic wastewater, J. Mol. Liq. 207 (2015) 216–223.
[41] V. Masindi, W.M. Gitari, T. Ngulube, Kinetics and equilibrium studies for removal of fluoride from underground water using cryptocrystalline magnesite, J. Water Reuse Desalin. 5 (2015) 282–292.
[42] R. Rusmin, B. Sarkar, Y. Liu, S. McClure, R. Naidu, Structural evolution of chitosan–palygorskite composites and removal of aqueous lead by composite beads, Appl. Surf. Sci. 353 (2015) 363–375.
[43] V. Masindi, W.M. Gitari, K.G. Pindihama, Adsorption of phosphate from municipal effluents using cryptocrystalline magnesite: complementing laboratory results with geochemical modelling, Desalin. Water Treat. (2015) 1–13.
[44] D.L. Parkhurst, C.A.J. Appelo, Users guide to Phreeqc (Version 2)—A computer program for speciation, batch-reactions, one-dimensional transport and inverse geochemical calculations, Water-Resour. Investig. Rep. (1999) 99–4259.
[45] V.V. Nasedkin, M.T. Krupenin, Y.G. Safonov, N.M. Boeva, S.V. Efremova, A.I. Shevelev, The comparison of amorphous (cryptocrystalline) and crystalline magnesites, Miner. Slov. 33 (2001) 567–574.
[46] D.L. Sparks, Environmental Soil Chemistry, Academic Press, 1995.
[47] H.H. Murray, Applied Clay Mineralogy: Occurrences, Processing and Applications of Kaolins, Bentonites, Palygorskitesepiolite, and Common Clays, Elsevier Science, 2006.
[48] B.J. Alloway, Heavy Metals in Soils, Chapman & Hall, 1990.
[49] T. Nkonyane, T. Ntuli, E. Muzenda, Treatment of acid mine drainage using unactivated bentonite and limestone, World Acad. Sci. Eng. Technol. 68 (2012) 139–144.
[50] R. Rusmin, B. Sarkar, Y. Liu, S. McClure, R. Naidu, Structural evolution of chitosan–palygorskite composites and removal of aqueous lead by composite beads, Appl. Surf. Sci. 353 (2015) 363–375.
[51] Dwaf, South African Water Quality Guidelines, 1 (1996).